Detection Lung Nodules Using Medical CT Images Based on Deep learning techniques

Ali Abdulwahhab Mohammed [1] ID ✉, *Ali H. Abdulwahhab *[2]* ID ✉, *Ibraheem Kasim Ibraheem[3]*
ID ✉

[1] Department of Remote Sensing, College of Remote Sensing & Geophysics, Al-Karkh University of Science, Baghdad, Iraq.
[2] Department of Electrical - Computer Engineering, College of Engineering, Altinbas University, Istanbul, Turkey.
[3] Department of Electrical Engineering, College of Engineering, Baghdad University, Baghdad, Iraq.
*Corresponding Author

Abstract

Lung nodule cancer detection is a critical and complex medical challenge. Accuracy in detecting lung nodules can significantly improve patient prognosis and care. The main challenge is to develop a detection method that can accurately distinguish between benign and malignant nodules and perform effectively under various imaging conditions. The development of technology and investment in deep learning techniques in the medical field make it easy to use Positron Emission Tomography (PET) and Computed Tomography (CT). Thus, this paper presents lung cancer detection by filtering the PET-CT image, obtaining the lung region of interest (ROI), and training using Convolution neural network (CNN)-Deep learning models for defending the nodules' location. The limitation dataset composed of 220 cases with 560 nodules with fixed Hounsfield Units (HU) is used to increase the training's speed and save data. The trained models involve CNN, DCNN, 3DCNN, VGG 19, ResNet 18, Inception V1, and Inception-ResNet to detect the lung nodules. The experiment shows high-speed training with VGG 19 outperforming the rest of deep learning, it achieves accuracy, Precision, Specificity, Sensitivity, F1-Score, IoU, FP rate with standard division; 98.65 ± 0.22, 98.80 ± 0.15, 98.70 ± 0.20, 98.55 ± 0.18, 98.60 ± 0.16, 0.94 ± 0.03, 1.05 ± 0.22, respectively. Moreover, the experiment results show an overall error rate and a standard division between ± 0.04 to ± 0.54 distributed over the calculation terms.

Keywords: Convolution Neural Network (CNN), CT image, Deep Learning, lung cancer, lung nodules.

Introduction

Lung cancer has grown to become one of the world's most dangerous diseases, killing thousands of people[1,2]. According to a 2020 report from the WHO, annually lung cancer causes 1.80 million deaths. Statistics such as these make lung cancer a very important direction for research in medicine[2,3]. Pulmonary nodules are often an early indication of lung cancer; however, not all of them are malignant.

The nodules need early detection and accurate segmentation for proper diagnosis and treatment[3]. Chest CT scan is one of the most common methods used to detect lung nodules. However, a single CT can produce hundreds of images that need analysis by a radiologist; this process becomes time-consuming and laborious. Image segmentation in analyzing characteristics—the shape, size, and

texture of the nodules—can help in assessing malignancy. This information is very important in lung cancer studies to assist in developing more personalized and precise diagnostic models[4]. In most cases, manual or semi-automatic segmentation is very time-consuming and sometimes marked by inconsistencies. On the other hand, automated detection and segmentation give fast results efficiently, reducing bias during the segmentation process[5]. Artificial intelligence and deep learning offer high accuracy in detection and information mining[6]. Deep learning has already found applications in various aspects of lung cancer imaging, such as tumor detection, CT scan segmentation, and image classification[6]. Nevertheless, most studies have been oriented towards just one task, like detection or segmentation, with variable quality[3,7]. The quality of the DL studies for the simultaneous detection and segmentation of lung nodules has not been analyzed until now. Conventional diagnostic methods, including visual inspection and biopsy, are time-consuming, subjective, and prone to missed diagnoses. Deep learning is a potent tool with the potential to transform cancer diagnosis[4,8]. DL algorithms learn patterns from large datasets that are imperceptible to the human eye. In the past few years, DL algorithms have been successfully demonstrated to be capable of performing better than human experts at cancer detection[9]. The achievements include improved diagnostic accuracy, decreased diagnosis costs, and an improved patient experience. There are problems associated with using DL for diagnosis: availability of data, bias, and transparency of the decision-making process. Big data, computing power, and innovations in neural network architectures have been the major driving forces for the recent advancement of DL, hence its application to medical diagnosis. DL algorithms show a remarkably high capability in detecting and classifying diseases in medical imaging, more so in cancer diagnosis[10]. Trained on large, heterogenous datasets of medical images, the DL algorithms can very effectively spot the smallest changes, which may be indicative of the growth of cancer, thus helping in its detection and intervention in the incipient stages[11]. In addition, DL has gone much ahead of the basic techniques that work on simple image-based methods by conglomerating multisource data; this is a specific

pointer toward greater accuracy in detection and diagnosis and thus a more personal and accurate approach to the management of disease[12]. New revolutionary possibilities of DL development in medical diagnosis, with an emphasis on lung cancer detection, are now real. DL does not just help with the early detection of cancer; it also holds promise for optimizing treatment outcomes and the quality of life. The development and integration of this technology into clinical practice serve as a critical step toward a more sophisticated and effective future of medical diagnosis[13].

Various studies have been conducted in this field. Candidates in this field, Seema et al[14], presented DLCT LUNG Detect Net using deep learning for detecting the lung nodules using CT images. Yan et al[15], developed a deep CNN model augmented with attention mechanisms to detect the lung nodules using overlap CT images. Alwyn et al[16], introduced 3D-VNet deep learning mothed for segmenting the pulmonary nodules, and designed 3D-ResNet model for classification of the nodules. Kumar et al[17], designed a hybrid DL model for predication and classification the lung nodules using CT images. Lip et al[18], used hybrid extraction feature approach composed of integration Gray-level cooccurrence matrix (GLCM) with Haralick and auto encoder features to detect lung cancer based on SVM and RBF techniques. Ahmed et al[5], discussed hybrid deep learning techniques that involved DCNN, VGG 19, and LSTMs to detect the lung cancer location. Shalini and Vigneshwari[9], developed a novel hybrid DL method involving 3D-CNN to detect lung nodules using database Consortium and Image Database Resource Initiative (LIDC-IDRI). Hafiz et al[19], designed 2D-ensemble model consisting of three CNN models to classify and detect the lung cancer using LUNA16 Grand challenge dataset. Mohamed et al[20], discussed the improvement of DL-based segmentation model to enhance the extraction features of CT images for detecting the lung cancer. Shafi et al[21], presented CAD deep learning model based on hybrid classifiers for prediction the segmented-ROI lung image-based extracted patches. Raut et al[22], discussed the detection of lung cancer using machine learning techniques based on segmented images. Rehman et al[23], presented the detection and classification of lung cancer based on

machine learning techniques that involving LBP, DCT, KNN, and SVM. Table 1, presents a summary of the related works.

Table 1. Summary of related works of lung cancer diagnosis

Ref	Tech	Accuracy	Precision	Specificity	Sensitivity	F1-Score
[14]	Hybrid DL model	97	100	N.A.	100	99
[15]	2DCNN-dual attention mechanism	95.40	95.80	93.17	94.69	95.24
[16]	3D-ResNet	99.2	N.A.	99.6	98.8	N.A.
[17]	LNDC-HDL	96.39	N.A.	96.12	95.25	N.A.
[18]	Hybrid (Haralick + (GLCM)	99.78	N.A.	99.72	99.82	N.A.
[5]	VGG-19 and LSTMs	99.75	99.42	N.A.	99.88	N.A.
[9]	CDCHNN	87	89	88	89	N.A.
[19]	Ensemble DL approach	95	N.A.	N.A.	N.A.	N.A.
[20]	Ensemble DL approach	96.2	97.4	98.4	98	98.4
[21]	CNN-based SVM	94	95	N.A.	94.5	94.5

There is a wide research gap in establishing how deep learning models relying on a few PET-CT images compare to those that were trained using large datasets. This therefore calls for testing how such a model will perform and generalizing when the resources available are limited. Thus, this study discusses the detection of lung nodules using limited collection of PET-CT images based deep learning techniques. The images are subjected to pre-process including removing borders, imitating of large airways, trachea, and blood vessels, and extracting the lung lobes from the lung image through the segmentation process by adopting the ROI to get a clear CT image from the impurities to improve the detection accuracy for the nodules

Methodology

This section highlights the most important contributions and recommended deep learning models that have been applied in the task of detecting lung Nodules using PET-CT Images. Fig 1, presents the framework of the lung nodule detection based on the PET-CT Images.
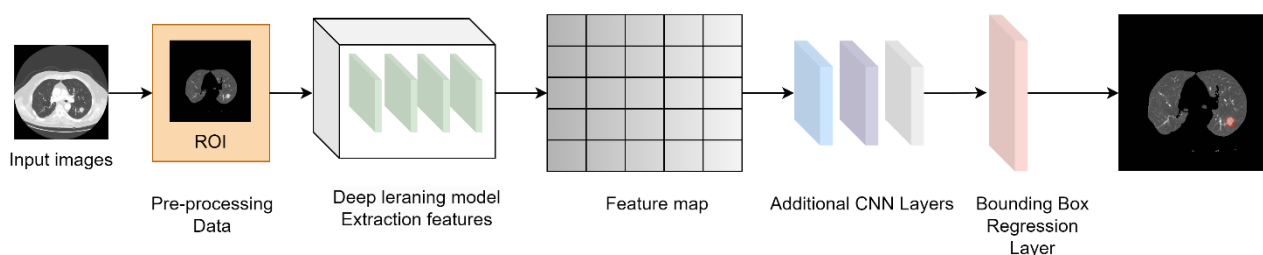

Figure 1. Framework of the lung nodules detection based on the PET-CT Images.

Pre-processing dataset

The CT image from Harbin's imaging data center is used in this experiment. PET-CT image data contains 220 cases with 560 nodules, and Fig 2 presents a few samples of the adopted CT image in the present study[24]. To enhance the detection accuracy of lung cancer, a series of pre-treatment steps were employed on the CT images. The initial step involved the removal of the CT image background to isolate the lung lobes. This process used a convolutional neural network (CNN), specifically the U-Net architecture[25], which is particularly effective in medical image segmentation due to its ability to capture both fine details and large contextual information. The U-Net model consists of an

encoder-decoder structure, where the encoder captures context through down-sampling, and the decoder enables precise localization through up-sampling. The segmentation process entailed several steps: first, the input CT images were resized and normalized to ensure uniformity; then, they were fed into the U-Net model, which produced binary masks highlighting the lung regions. Further, binary masks obtained after segmentation were smoothened using morphological operations like erosion and dilation to avoid small artifacts and provide smooth lung boundaries. After the refinement of the masks with the aid of morphological operations, connected component analysis was done to isolate lung regions.

Immediately following segmentation, another critical step involved the extraction of regions of interest. This step involved the isolation of lung tissue from other anatomical structures so that analyses were focused on areas relevant to lung cancer detection. Processed ROIs were then extracted using different image processing techniques that enhance the visibility of the nodules of interest. The steps included histogram equalization for contrast and edge detection to outline nodule boundaries. These ROIs were fed into a deep convolutional neural network trained for lung nodule detection to identify nodules with diameters between 3 mm and 30 mm.
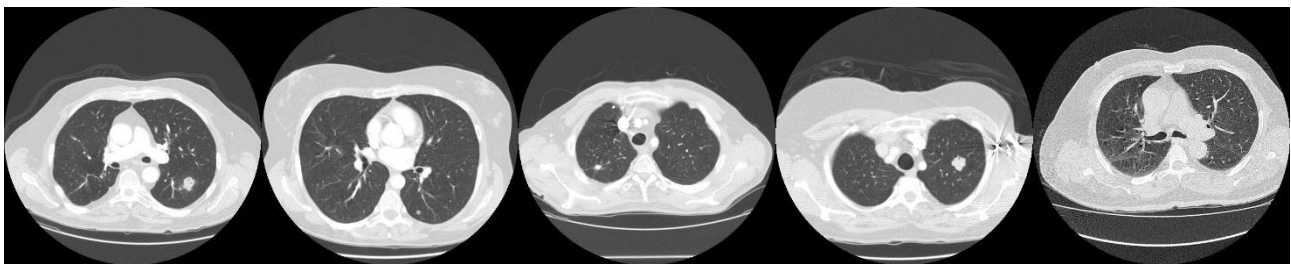

Figure 2. Dataset CT-images samples.

The formula for calculating the gradient estimation of the lung nodule's location is given;

$$\Delta w \leftarrow \frac{1}{|b|} \sum_{x^{(i)} \in b} \nabla_w J^i(x, w) \qquad 1$$

Update weight:

$$w \leftarrow w - \varepsilon \, \Delta w$$

End while

where ε is the learning rate, and Δw is the computed gradient. b is the batch size, $x^{(i)}$ is input data, $\nabla_w J^i(x, w)$ is the gradient loss function.

Convolutional Neural Network

The Convolutional Neural Network is another class of deep neural networks characterized by the use of convolutional layers, replacing the fully connected traditional neural network layers. This kind of structure with spatially stable and weight-shared treatment deals efficiently with processing and pattern recognition in image data; hence, appropriate to realize image classification and segmentation tasks[26,27]. In general, there are three main layers of CNN: the convolution layer, the pooling layer, and actuation. In CNN, there is a stack of convolution layers and a pooling layer followed by the actuation layer. The most critical layer is the convolution layer, which is the convolution task. The convolution layer contains channels with learning abilities called convolution layer's components. These channels work as filters of a square matrix and have locative length, width, and depth. These filters cover the full information volume. The pooling layer is located between the convolution layers. It is an essential layer in the structure system if the procced image is more significant, and the amenable components can be considerable. This takes time to prepare the network system and is impractical. The pooling layer is adopted to reduce the image's span. There are several layers; the max pooling layer is the most used. The Productive CNN neural networks are widely used in image recognition and processing,

speech recognition, recommendation systems[28], language recognition analysis[29], and classification of images[30,31], Face detection[32]. The general CNN structure diagram is shown in Fig 3.
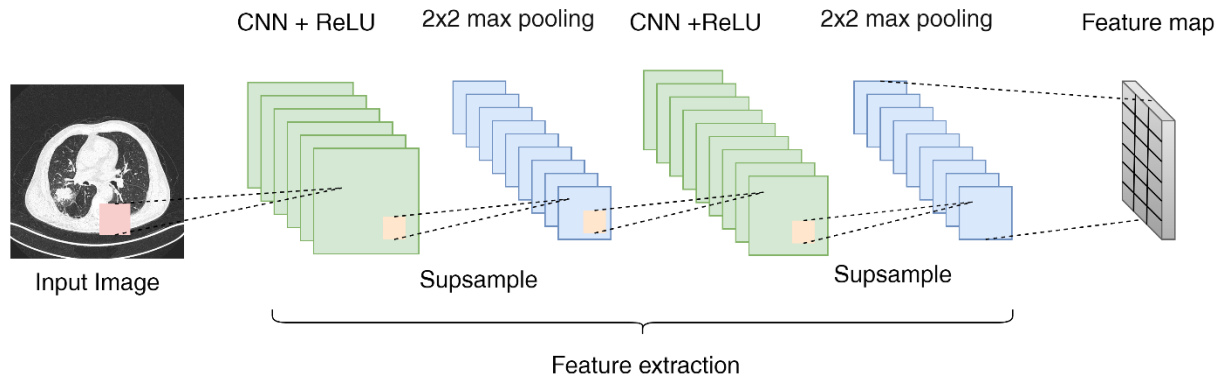

Figure 3. The CNN structure diagram.

Deep Convolution Neural Network (DCNN)

Deep Convolution Neural Network (DCNN) is a neural network that belongs to the multiple-layer classification[33]. The traditional neural network mainly adopts a layer-to-layer connection architecture mode; in turn, the networks adopt sparse connections[34]. DCNN has deeply analyzed the correlation between the neural layers and significantly affects the processing and extraction of causal data[35]. The parameters of adopted network layers, such as bias terms and weight matrix, are the same for each layer and are built by combining convolutional layers and pooling layers. The number of layers is relatively large. The weight-sharing mode feature has the most significant advantage; it effectively reduces the parameters in the network architecture and dramatically reduces the computational cost in the network. The structural feature diagram is shown in Fig 4. CT image is subjected to feature extraction calculation to obtain the feature map of the input terminal. The adopted DCNN uses the gradient descent method to reduce losing data in the calculation feature by reversely adjusting each parameter and adopting multiple iterative training methods to strengthen the training ability of the neural network. Thus, the CT image is changed from 512 x 512 px to 260 x 260 px to reduce the degree of image calculation and improve calculation efficiency. The formula for a forward propagation network is given as follows;

$$H_i^l(u_1, u_2) = \sigma\left(B_i^l + \sum_k \sum_{v_1,v_2} H_k^{l-1}\right)(u_1 - v_1, u_2 - v_2)w_{ki}^l(v_1, v_2,) \qquad 2$$

where H_i^l is the output of l at layer i, H_k^{l-1} is the output of l when layer ki goes upper in the network, (u_1, u_2) are dimensional of the network, w_{ki}^l is the weight of the convolution kernel (v_1, v_2) is the two different dimensions of w, B_i^l is the bias, and σ is the nonlinear activation function. Assuming that the input value of the initial layer is x and the output value is y, then;

$$y = f(x, w) \qquad 3$$

The loss function is as follows:

$$J(x, w) = \sum_{i=1}^m J^i(x, w) \qquad 4$$

where m is the number of training samples. The stochastic gradient descent algorithm follows: Let the learning rate be ε, and the initial weight is w.
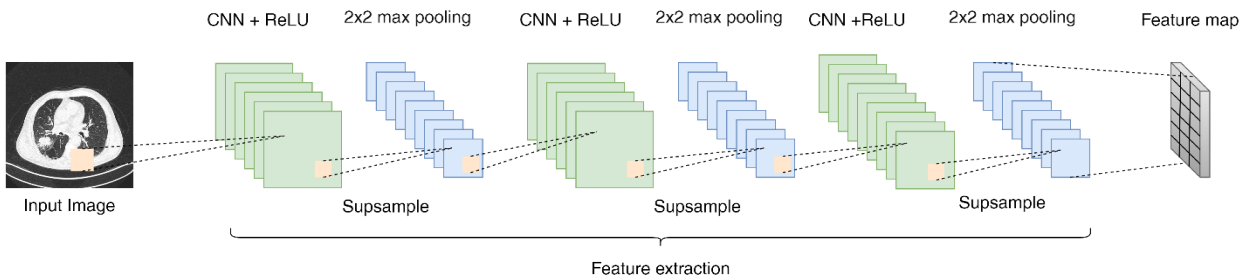
Figure 4. DCNN structure diagram.

3D-Convolutional Neural Network (3DCNN)

3D-Convolution captures the image dimension and the spatial data information more effectively than traditional CNN. 3D-CNN's dimension is 3 to process the medical image[36]. The 3D-CNN operation is performed on the three continuous frames of an image and captures multiple continuous frames to generate a cube. The convolution kernel is adopted to calculate the cube's frames. The structural feature diagram of 3D-CNN is presented in Fig 5. The feature map is connected into multiple consecutive frames related to the previous layer to capture motion information. The 3D-CNN kernel allows only one feature to be extracted from the cube due to the shared weight in the neural network. 3D CNN works on selecting a center point in the nodule as a coordinate, which is surrounded by a small cube with dimensional 16 x 16 x 16 px as output. The calculation formula of 3D CNN is as given as follows;

$$H_i^l(u_1, u_2, u_3) = \sigma \left(B_i^l + \sum_k \sum_{v_1, v_2, v_3} H_k^{l-1} \right)(u_1 - v_1, u_2 - v_2, u_3 - v_3) w_{ki}^l (v_1, v_2, v_3) \quad 5$$
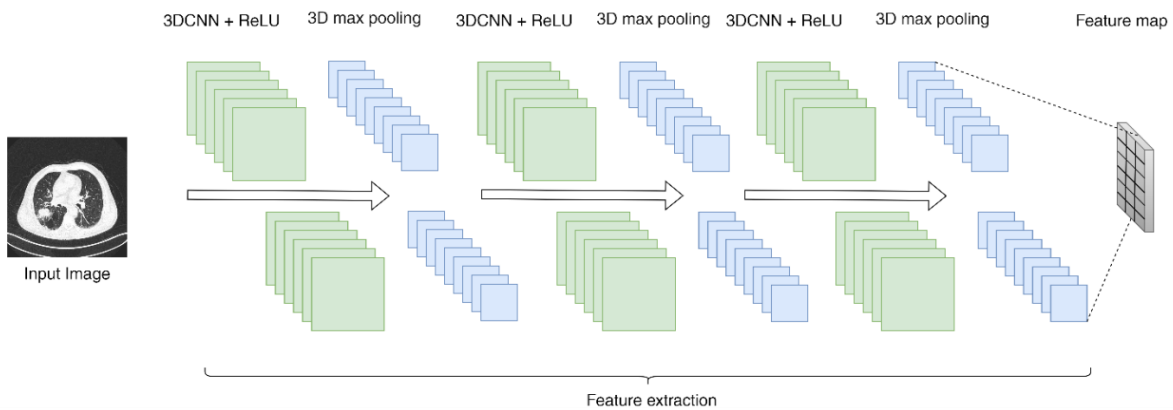

Figure 5. 3DCNN structure diagram.

VGG 19

VGG19 is a convolutional neural network (CNN) model developed by a team from the Visual Geometry Group (VGG) at the University of Oxford [37]. The model is known for its simple yet deep architecture, consisting of 19 layers in total, including 16 convolutional layers and 3 fully connected layers. VGG19 is a variant of VGG, where the number 19 indicates the total number of learning layers. Fig 6, presents the VGG 19 deep learning model architecture diagram
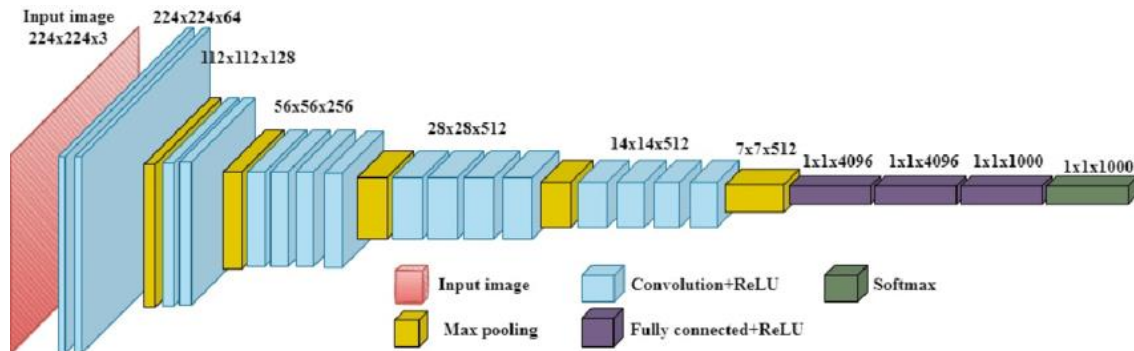
Figure 6. VGG 19 structure diagram[38].

The VGG19 architecture uses convolutional layers with a fixed filter size of 3x3, which is considered optimal for capturing complex visual patterns. After each convolutional layer, there is a ReLU (Rectified Linear Unit) non-linearity layer that helps in introducing non-linearity into the model. After multiple convolution blocks, there will be a max-pooling layer with a filter size of 2x2, along with a stride of 2 to reduce the spatial dimensionality of the feature map. At the very end of the model, add a fully connected layer for two layers containing 4096 units and one output layer containing a number of units equal to the number of classes involved in a particular classification task. VGG19 has been applied to many image recognition and image segmentation and detection tasks. It is also often used as a basis for more complex deep learning models via transfer learning.

ResNet 18

ResNet18 is a variant of Residual Networks (ResNet), introduced by Kaiming He and colleagues in 2015[39]. ResNet18 consists of 18 layers, including 17 convolutional layers, and one fully connected layer. One of the main innovations of the ResNet architecture is the introduction of residual blocks, which allow gradients to flow better through the deep network, thus solving the vanishing gradient problem that often occurs in very deep neural networks. Fig 7 presents the ResNet18 deep learning model architecture diagram.
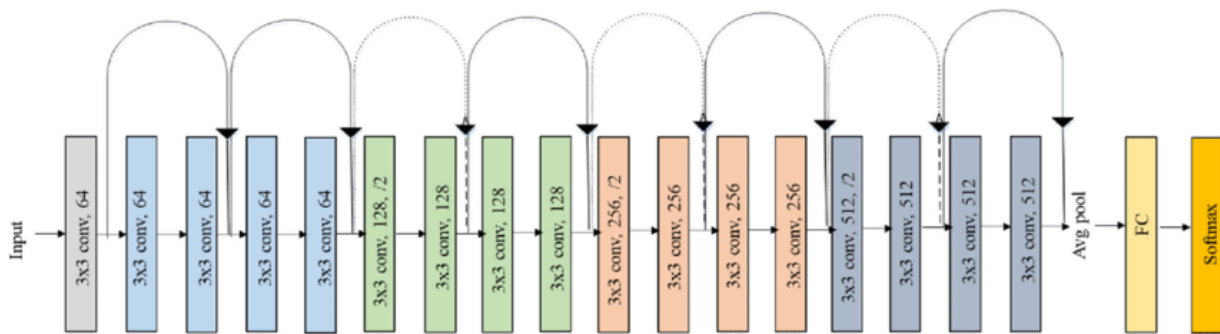

Figure 7. ResNet 18 structure diagram[40].

ResNet's residual blocks consist of shortcut connections that connect the input directly to the output of several layers ahead. This structure allows the network to learn identity mapping, which makes it easier to train models with hundreds or even thousands of layers. In ResNet18, each residual block consists of two convolutional layers with a filter size of 3x3, followed by batch normalization and ReLU activation. The ResNet18 architecture generally consists of an initial convolutional layer, followed by four residual blocks, and ending with a fully connected layer. Each residual block is usually followed by a pooling layer to reduce the spatial dimension. ResNet18 is known for its balance between depth and computational complexity, making it widely used in various applications such as object recognition, object detection, and image segmentation.

Inception v1

Inception v1, also known as GoogLeNet, is a CNN model introduced by the Google team in 2014[41]. It introduced the concept of Inception modules, which allow combining

different sizes of convolutional filters in a single layer, thus increasing the network's ability to capture different

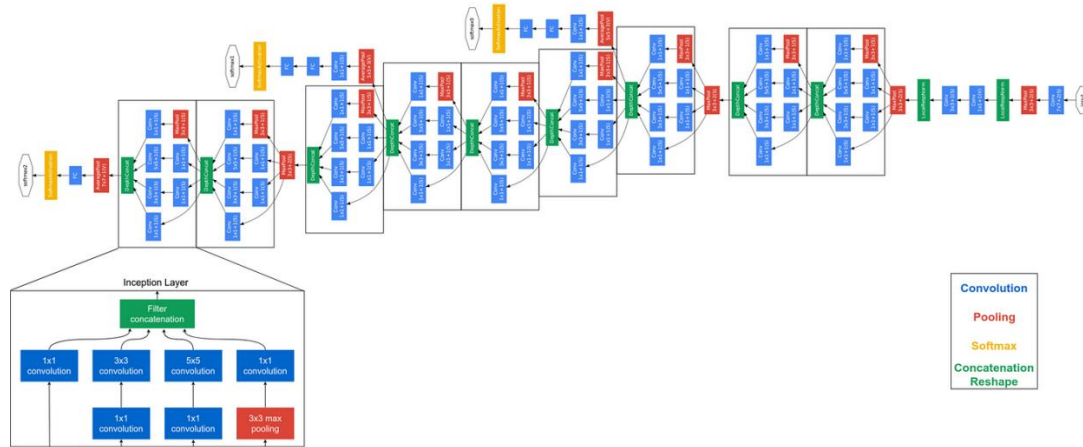types of features in an image. Fig 8, presents the Inception v1 deep learning model architecture diagram

Figure 8. Inception v1 structure diagram[42].

Each Inception module in Inception v1 consists of multiple parallel paths that perform convolution operations with different filter sizes (1x1, 3x3, 5x5) as well as a pooling path. The outputs of each of these paths are then concatenate to form the final output of the module. This allows the model to extract features from different scales simultaneously, which is very useful for identifying complex visual features. The Inception v1 architecture consists of 22 layers with multiple Inception modules. The model also uses an auxiliary classifier layer placed before the final layer to aid training and mitigate the vanishing gradient problem. Inception v1 has been

widely used in various computer vision applications and is often the basis for newer Inception architectures.

Inception-ResNet

Inception-ResNet is created by crossing two of the most popular architectures in deep learning: Inception and ResNet. It retains the advantages of Inception modules and residual blocks to give a more efficient and easily trained network. Inception-ResNet was introduced to overcome some of the drawbacks of the Inception and ResNet architectures separately[43]. Fig 9, presents the Inception-ResNet v1 deep learning model architecture diagram.
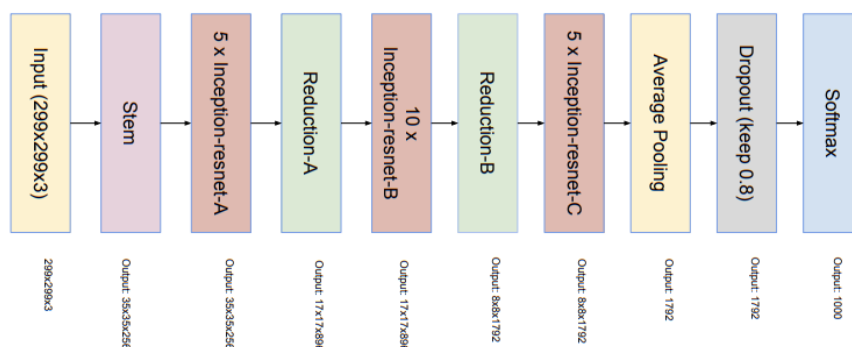

Figure 9. Inception-ResNet v1 structure diagram[44].

Inception-ResNet uses a modified Inception module by adding shortcut connections as in ResNet. Each module in Inception-ResNet consists of several parallel

convolutional paths with different filter sizes, similar to Inception v1. However, the outputs of these paths are added to the original inputs (shortcuts) using a sum

operation, similar to the concept of ResNet residual blocks. The main advantage of Inception-ResNet is its ability to maintain the computational efficiency of Inception modules while taking advantage of the better training stability and gradients of residual blocks. This model usually consists of several Inception-ResNet modules, followed by convolutional and fully connected layers. Inception-ResNet has shown superior performance in various image recognition tasks and is often used in computer vision competitions.

Results and Discussion

PET-CT image pre-treatment

Usually, the PET-CT image is prone to steady noise. Thus, The CT image's HU (HU is a unit describing x-ray intensity) is limited to be between -1000 to –400 for the pre-processing step. In the pre-processing stage, CT images undergo a series of enhancements to filter out noise and other irrelevant influences, thereby improving the quality of the data used for training and lung abnormality detection. First, CT images are resized to be consistent and normalized to a standard range (e.g. 0-1) based on the Hounsfield Unit (HU) scale. This normalization helps stabilize the training process and ensures that the model receives input with a consistent range, making it easier to learn meaningful patterns. Next, to reduce the impact of noise and improve the quality of lung regions for further analysis, a Gaussian filter and grayscale masks are used to smooth the images, which helps reduce random noise by averaging pixel values with their neighbors. After noise reduction, histogram equalization is applied to improve image

Evaluation matrix

The performance of the detection deep learning models is evaluated based on the following items[26]:

- Accuracy: (TP + TN) / (TP +TN +FB +FN)
- Precision: TP / (TP + FP)
- Sensitivity: TP / (TP + FN)
- Specificity: TN / (TN + FP)
- F1-score: 2 * ((Precision* Sensitivity) / (Precision + Sensitivity))
- IoU: Area of overlap / Area of union[45]

contrast, making features such as lung nodules easier to recognize. After the histogram equalization, binary segmentation is applied. Morphological operations such as erosion and dilation are used to refine the boundaries of the segmented lung regions, ensuring that they correspond to the actual anatomical structures. Connected component analysis is then performed to accurately isolate each lung region, even if they are adjacent or partially overlapping. Finally, edge detection techniques, such as the Canny edge detector, are used to highlight the boundaries of potential nodules in the lung tissue for the obtained lung ROI, making it easier for the deep convolutional neural network (DCNN) to identify and detect these features. Fig 10 shows the outcomes of the pre-processing approach of the images before detection of the lung Nodules using DCNN models. These comprehensive pre-processing steps are essential to filter out irrelevant information and improve the quality of CT images, thereby increasing the accuracy and efficiency of the lung cancer detection process.

Figure 10. Pre-processing PET-CT lung, (a) original lung PET-CT image, (b) Gaussian filter - gray scale masked PET-CT image, (c) CT image after binary segmentation, (d) Independent segmented lung lobe after removing borders, (e) Independent lung lobe after limitation large airways, trachea, and blood vessels, (f) Independent lung lobe image.

Performance Deep learning models

In Table 2, the detection performance of various deep learning models on PET-CT images is presented with metrics such as accuracy, precision, sensitivity, F1 score, IoU, and false positive rate (FP Rate), along with standard deviation (± SD). Standard deviation (SD) measures the extent to which individual values of the metric are spread out or vary from the mean. The VGG19 model shows a clear advantage in this regard. With the highest accuracy of 96.35% ± 0.28, this means that the average detection accuracy of VGG19 is 98.65%, and the results from different experiments usually vary by about 0.22 percentage points above or below the mean. The small standard deviation indicates that the detection result of VGG19 is consistent and reliable. For example, the precision of VGG19 is 98.80 ± 0.15, which indicates that although the average accuracy of precision is 98.80 %, the result of different experiments may differ by about 0.15 percentage points. The high

sensitivity, 98.55 ± 0.18, reflects that the results are good not only on average but also stable in the detection of positive cases; this can be shown by the standard deviation expressing the variation of results around the mean value. VGG19 had an F1 score of 98.60 ± 0.16, demonstrating that it can maintain an excellent balance between precision and sensitivity with a small variation of results around the mean value. The IoU index of VGG19 is the highest among the models: 0.94 ± 0.03, indicating very good detection of relevant areas, and a small standard deviation means consistency in quality. In addition, the false positive rate of VGG19 is the lowest at 0.97, thereby avoiding false detection. Overall, VGG19's superiority in accuracy, precision, sensitivity, F1 score, as well as its small standard deviation and low false positive rate indicates it's very superior detection performance compared to other models in the table. Fig 11 shows a sample of detection lung nodules using PET-CT image based on VGG 19 deep learning model.

Table 2. The comparison between adopted techniques

Technical	Accuracy (±SD)	Precision (±SD)	Specificity (±SD)	Sensitivity (±SD)	F1-Score (±SD)	IoU (±SD)	FP rate (±SD)
CNN	84.45 ± 0.54	93.14 ± 0.37	86.33 ± 0.21	81.20 ± 0.45	86.79 ± 0.32	0.68 ± 0.04	2.89 ± 0.30
D-CNN	90.32 ± 0.44	97.23 ± 0.11	91.14 ± 0.27	89.01 ± 0.39	93.99 ± 0.24	0.76 ± 0.03	2.03 ± 0.28
3D-CNN	93.21 ± 0.54	98.43 ± 0.45	92.31 ± 0.43	91.40 ± 0.47	94.85 ± 0.34	0.81 ± 0.04	1.47 ± 0.25
VGG19	98.65 ± 0.22	98.80 ± 0.15	98.70 ± 0.20	98.55 ± 0.18	98.60 ± 0.16	0.94 ± 0.03	1.05 ± 0.22
ResNet 18	92.14 ± 0.42	97.90 ± 0.28	91.87 ± 0.34	90.56 ± 0.40	94.19 ± 0.30	0.79 ± 0.04	1.80 ± 0.26
Inception v1	91.32 ± 0.47	97.45 ± 0.32	91.14 ± 0.39	89.78 ± 0.43	93.60 ± 0.29	0.75 ± 0.05	1.98 ± 0.28
Inception-ResNet	93.03 ± 0.38	98.21 ± 0.25	92.45 ± 0.31	91.12 ± 0.35	94.63 ± 0.27	0.80 ± 0.04	1.85 ± 0.24
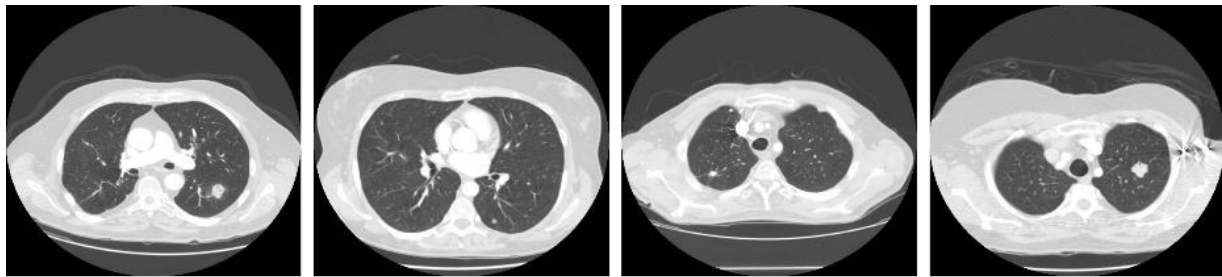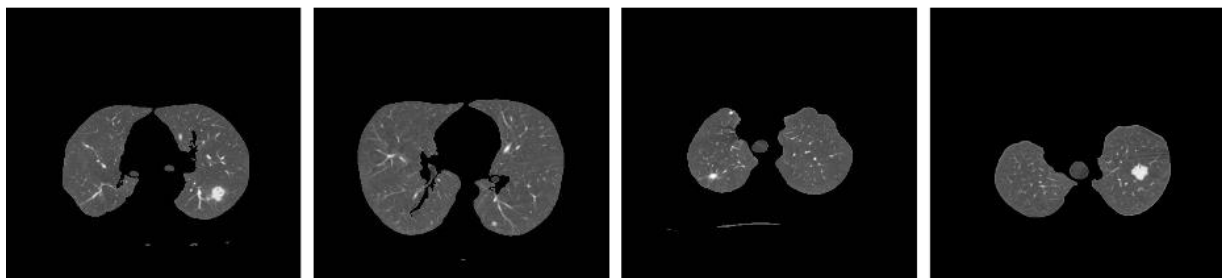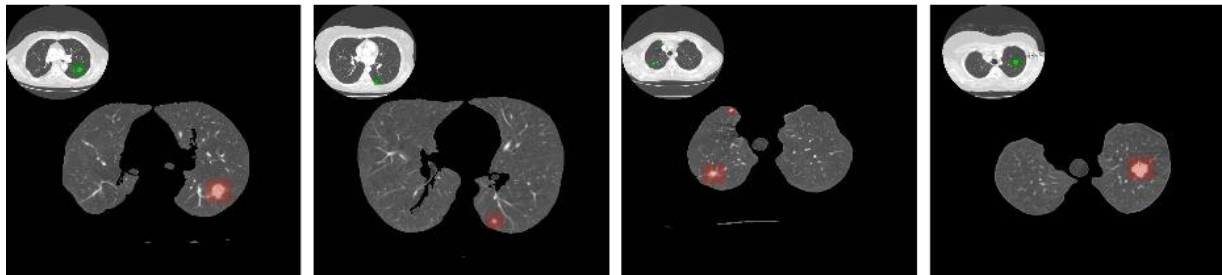
Figure 11 samples of Lung nodules detection based on ROI (a) Initial CT image (b) Independent CT image (c) Independent CT image nodules' location detection.

Conclusion

In this study the detection of lung nodules based on segmented ROI using deep learning techniques is discussed. The dataset is collected from Harbin's imaging data center, and prepared with limited HU (HU is a unit describing x-ray intensity between -1000 to – 400 for pre-processing. The image processing involves filtering, and segmenting to remove the borders and limit the large airways, trachea, and blood vessels to obtain the ROI lung represented by the Independent lung lobe image. Pre-trained deep learning models are used to execute this experimental, CNN, DCNN, 3DCNN, VGG 19, ResNet 18, Inception V1, Inception-ResNet v1, the resulting features map of these models are connected with three CNN layers followed by bounding box regression layer to determine the location of the lung nodules with diameters between 3 mm and 30 mm. The experiment showed the superiority of the VGG 19 model with 98.65% detection accuracy. In future work, the developed model involved attention mechanism transformation integrated with deep learning technique to segment lung nodules and define nodules' size -based classes, in this way we can classify lung cancer based on nodules' size.

Authors' Declaration

- Conflicts of Interest: None.
- We hereby confirm that all the Figures and Tables in the manuscript are ours. Furthermore, any Figures and images, that are not ours, have been included with the necessary permission for re-publication, which is attached to the manuscript.

- No animal studies are present in the manuscript.
- No human studies are present in the manuscript.
- Ethical Clearance: The project was approved by the local ethical committee at Altinbas University, Istanbul, Turkey.

Authors' Contribution Statement

A.H.A proposed the idea, collected data, and drafted the initial paper, designing the structure of the article. Then, A.A.M took responsibility for reviewing and editing the content, ensuring clarity and consistency, as well as carefully checking the language accuracy. Based on their efforts, I.K.I meticulously reviewed the paper, focusing carefully on references, and carefully searching for signs of plagiarism.

References

1. Hosseini SH, Monsefi R, Shadroo S. Deep learning applications for lung cancer diagnosis: a systematic review. Multimed Tools Appl. 2024 Mar 15; 83(5): 14305-14335. https://doi.org/10.1007/s11042-023-16046-w.

2. Abdulwahhab AH, Mahmood NT, Mohammed AA, Myderrizi I, Al-Jumaili MH. A Review on Medical Image Applications Based on Deep Learning Techniques. J Image Graph. 2024 July; 12(3): 215-227. https://doi.org/10.18178/joig.12.3.215-227.

3. Gayap HT, Akhloufi MA. Deep machine learning for medical diagnosis, application to lung cancer detection: a review. BioMedInformatics. 2024 Jan; 4(1): 236-284. https://doi.org/10.3390/biomedinformatics4010015.

4. Thanoon MA, Zulkifley MA, Mohd Zainuri MA, Abdani SR. A review of deep learning techniques for lung cancer screening and diagnosis based on CT images. Diagnostics. 2023 Aug; 13(16): 2617. https://doi.org/10.3390/diagnostics13162617.

5. Alsheikhy AA, Said Y, Shawly T, Alzahrani AK, Lahza H. A CAD system for lung cancer detection using hybrid deep learning techniques. Diagnostics. 2023 Mar; 13(6): 1174. https://doi.org/10.3390/diagnostics13061174.

6. Chiu HY, Chao HS, Chen YM. Application of artificial intelligence in lung cancer. Cancers. 2022 Mar 1; 14(6): 1370. https://doi.org/10.3390/cancers14061370.

7. Gao Q, Yang L, Lu M, Jin R, Ye H, Ma T. The artificial intelligence and machine learning in lung cancer immunotherapy. J Hematol Oncol. 2023 May; 16(1): 55. https://doi.org/10.1186/s13045-023-01456-y.

8. Davri A, Birbas E, Kanavos T, Ntritsos G, Giannakeas N, Tzallas AT, et al. Deep learning for lung cancer diagnosis, prognosis and prediction using histological and cytological images: a systematic review. Cancers. 2023 Aug; 15(15): 3981. https://doi.org/10.3390/cancers15153981.

9. Wankhade S, Vigneshwari S. A novel hybrid deep learning method for early detection of lung cancer using neural networks. Healthc Anal. 2023 Nov 1; 3: 100195. https://doi.org/10.1016/j.health.2023.100195.

10. Rajasekar V, Vaishnnave MP, Premkumar S, Sarveshwaran V, Rangaraaj V. Lung cancer disease prediction with CT scan and histopathological images feature analysis using deep learning techniques. Results Eng. 2023 Jun 1; 18: 101111. https://doi.org/10.1016/j.rineng.2023.101111.

11. Deepapriya BS, Kumar P, Nandakumar G, Gnanavel S, Padmanaban R, Anbarasan AK, et al. Performance evaluation of deep learning techniques for lung cancer prediction. Soft Comput. 2023 Jul; 27(13): 9191-9198. https://doi.org/10.1007/s00500-023-08313-7.

12. Forte GC, Altmayer S, Silva RF, Stefani MT, Libermann LL, Cavion CC, et al. Deep learning algorithms for diagnosis of lung cancer: a systematic review and meta-analysis. Cancers. 2022 Aug; 14(16): 3856. https://doi.org/10.3390/cancers14163856.

13. Zhang P, Xu X, Wang H, Feng Y, Feng H, Zhang J, et al. Computer-aided lung cancer diagnosis approaches based on deep learning. J Comput Aided Des Comput Graph. 2018 Jan; 30(1): 90-99. https://doi.org/10.3724/SP.J.1089.2018.16919.

14. Rathod SB, Ragha LL. DLCT LUNG Detect Net: Leveraging Deep Learning for Lung Tumor Detection in CT scans. J Electr Syst. 2024; 20(2s): 1290-1308. https://doi.org/10.52783/jes.1771.

15. UrRehman Z, Qiang Y, Wang L, Shi Y, Yang Q, Khattak SU, et al. Effective lung nodule detection using deep CNN with dual attention mechanisms. Sci Rep. 2024; 14(1): 3934. https://doi.org/10.1038/s41598-024-51833-x.

16. Crasta LJ, Neema R, Pais AR. A novel Deep Learning architecture for lung cancer detection and diagnosis from Computed Tomography image analysis. Healthc Anal. 2024 Jun; 5: 100316. https://doi.org/10.1016/j.health.2024.100316.

17. Gugulothu VK, Balaji S. An early prediction and classification of lung nodule diagnosis on CT images based on hybrid deep learning techniques. Multimed Tools Appl. 2024 May; 83(1): 1041-1061. https://doi.org/10.1007/s11042-023-15802-2.

18. Li L, Yang J, Por LY, Khan MS, Hamdaoui R, Hussain L, et al. Enhancing lung cancer detection through hybrid features and machine learning hyperparameters optimization techniques. Heliyon. 2024 AFeb; 10(4): e26192.
https://doi.org/10.1016/j.heliyon.2024.e26192.

19. Shah AA, Malik HAM, Muhammad A, Alourani A, Butt ZA. Deep learning ensemble 2D CNN approach towards the detection of lung cancer. Sci Rep. 2023 Feb; 13(1): 2987. https://doi.org/10.1038/s41598-023-29656-z.

20. Shakeel PM, Burhanuddin MA, Desa MI. Automatic lung cancer detection from CT image using improved deep neural network and ensemble classifier. Neural Comput Appl. 2022 Apr; 1-14. https://doi.org/10.1007/s00521-020-04842-6.

21. Shafi I, Din S, Khan A, De La Torre Díez I, Palí Casanova RJ, Pifarre KT, et al. An effective method for lung cancer diagnosis from CT scan using deep learning-based support vector network. Cancers. 2022 Nov; 14(21): 5457. https://doi.org/10.3390/cancers14215457.

22. Raut S, Patil S, Shelke G. Lung cancer detection using machine learning approach. Int J Adv Sci Res Eng Trends. 2021 Jan; 6(1): 47-51. https://doi.org/0.51319/2456-0774.2021.0005.

23. Rehman A, Kashif M, Abunadi I, Ayesha N. Lung cancer detection and classification from chest CT scans using machine learning techniques. 1st International Conference on Artificial Intelligence and Data Analytics (CAIDA). 2021 (pp. 101-104). IEEE. https://doi.org/10.1109/CAIDA.2021.10059.

24. Li P, Wang S, Li T, Lu J, HuangFu Y, Wang D. A Large-Scale CT and PET/CT Dataset for Lung Cancer Diagnosis (Lung-PET-CT-Dx) [Data set]. Cancer Imag Arch. 2020. https://doi.org/10.7937/TCIA.2020.NNC2-0461.

25. Falk T, Mai D, Bensch R, Çiçek Ö, Abdulkadir A, Marrakchi Y, et al. U-Net: deep learning for cell counting, detection, and morphometry. Nat Methods. 2019 Jan; 16(1): 67-70. https://doi.org/10.1038/s41592-018-0261-2.

26. Abdulwahhab AH, Abdulaal AH, Al-Ghrairi AH, Mohammed AA, Valizadeh M. Detection of epileptic seizure using EEG signals analysis based on deep learning techniques. Chaos Solitons Fractals. 2024 Apr 1; 181: 114700. https://doi.org/10.1016/j.chaos.2024.114700.

27. Du D, Gu J, Chen X, Lv W, Feng Q, Rahmim A, et al. Integration of PET/CT radiomics and semantic features for differentiation between active pulmonary tuberculosis and lung cancer. Mol Imaging Biol. 2021 Apr; 23: 287-98. https://doi.org/10.1007/s11307-020-01550-4.

28. Ziyad SR, Radha V, Vayyapuri T. Overview of computer aided detection and computer aided diagnosis systems for lung nodule detection in computed tomography. Curr Med Imag. 2020 Jan 1; 16(1): 16-26. https://doi.org/10.2174/15734056156666190206153321.

29. Adeyanju IA, Bello OO, Adegboye MA. Machine learning methods for sign language recognition: A critical review and analysis. Intell Syst Appl. 2021 Nov 1; 12: 200056. https://doi.org/10.1016/j.iswa.2021.200056.

30. Mohammed AA, Khamees HT. Categorizing and measurement satellite image processing of fire in the forest Greece using remote sensing. Indones J Electr Eng Comput Sci. 2021 Feb; 21(2): 843-853. http://doi.org/10.11591/ijeecs.v21.i2.pp846-853.

31. Mohammed AA, Al-Ghrairi AH, Al-zubidi AF, Saeed HM. Unsupervised classification and analysis of Istanbul-Turkey satellite image utilizing remote sensing. AIP Conf Proc. 2023. AIP Publishing. https://doi.org/10.1063/5.0118339.

32. Al-Ghrairi AH, Mohammed AA, Sameen EZ. Face detection and recognition with 180-degree rotation based on principal component analysis algorithm. IAES Int J Artif Intell. 2022 Jun 1; 11(2): 593. https://doi.org/10.11591/ijai.v11.i2.

33. Singhal A, Phogat M, Kumar D, Kumar A, Dahiya M, Shrivastava VK. Study of deep learning techniques for medical image analysis: A review. Mater Today Proc. 2022 Jan 1; 56: 209-14. https://doi.org/10.1016/j.matpr.2022.04.081.

34. Jyoti V, Patel D, Pandya S, Sharma M, Patel J. Deep learning-based transfer learning model for early diagnosis of lung cancer. In 2018 IEEE International Conference on Signal Processing, Computing and Control (ISPCC). 2018 Sep 21 (pp. 232-237). IEEE. https://doi.org/10.1109/SPACES.2018.8316363.

35. Srinivasu PN, SivaSai JG, Ijaz MF, Bhoi AK, Kim W, Kang JJ. Classification of skin disease using deep learning neural networks with MobileNet V2 and LSTM. Sensors. 2021 May 14; 21(8): 2852. https://doi.org/10.3390/s21082852.

36. Dey N, Ashour AS, Shi F, Fong SJ, Sadiq AS, Sherratt RS. Developing residential wireless sensor networks for ECG healthcare monitoring. IEEE Trans Consum Electron. 2017 Jan; 63(4): 442-9. https://doi.org/10.1109/TCE.2017.015011.

37. Shahin M, Mohsen A, Al-Ghrairi AH, Saeed HM. Surface to image transmission, processing and classification. Indones J Electr Eng Comput Sci. 2020 Apr 1; 18(2): 843-853. https://doi.org/10.11591/ijeecs.v18.i2.pp843-853.

38. Solovyev R, Wang W, Gabruseva T. Weighted boxes fusion: Ensembling boxes for object detection models. Image Vis Comput. 2021 Oct 1; 107: 104117. https://doi.org/10.1016/j.imavis.2021.104117.

39. Shadroo S, Monsefi R, Hosseini SH. Epileptic seizure detection using convolutional neural networks based on electroencephalography signals: A comprehensive review. Comput Methods Programs Biomed. 2024 Jan; 222: 106992. https://doi.org/10.1016/j.cmpb.2022.106992.

40. Mohammed AA, Al-Ghrairi AH, Shadroo S, Hosseini SH. Deep learning-based epileptic seizure detection in EEG signals: a review. Appl Sci. 2024 Jan; 14(1): 301. https://doi.org/10.3390/app14010301.

41. Hosseini SH, Azari MA, Monsefi R, Shadroo S. Recent Advances in Machine Learning and Its Applications: A Comprehensive Review. J Artif Intell Res. 2023 Sep; 67: 53-91. https://doi.org/10.1613/jair.1.14061.

42. Nandhini N, Udhayakumar A, Balaji K, Alagarsamy P. Automated skin lesion classification using ensemble of deep learning models. Multimed Tools Appl. 2023 Jun 1; 82(3): 10741-10761. https://doi.org/10.1007/s11042-023-13675-0.

43. Prasad A, Gupta B. Survey on automated lung nodule detection in computed tomography images using deep learning techniques. Healthc Anal. 2024 Jan 1; 6: 100430. https://doi.org/10.1016/j.health.2023.100430.

44. Roy S, Menapace W, Oei S, Luijten B, Fini E, Saltori C, et al. Deep learning for classification and localization of COVID-19 markers in point-of-care lung ultrasound. IEEE Trans Med Imaging. 2020 Aug; 39(8): 2676-2687. https://doi.org/10.1109/TMI.2020.2994459.

45. Sarker IH. AI-based modeling: Techniques, applications, and research issues towards automation, intelligent, and smart systems. SN Comput Sci. 2022 Feb 21; 3(2): 158. https://doi.org/10.1007/s42979-022-01063-5 .

اكتشاف عقيدات الرئة باستخدام صور الأشعة المقطعية الطبية المعتمدة على تقنيات التعلم العميق

علي عبدالوهاب محمد1، علي حسين عبدالوهاب2، ابراهيم قاسم ابراهيم3

1قسم التحسس النائي، كلية التحسس النائي والجيوفيزياء، جامعة الكرخ للعلوم، بغداد، العراق..
2قسم الهندسة الكهربائية ـ الحاسوب، كلية الهندسة، جامعة التان باش، إسطنبول، تركيا.
3قسم الهندسة الكهربائية، كلية الهندسة، جامعة بغداد، بغداد، العراق.

الخلاصة

يعد اكتشاف سرطان عقيدات الرئة تحديًا طبيًا بالغ الأهمية ومعقدًا. يمكن أن يؤدي الدقة في اكتشاف عقيدات الرئة إلى تحسين تشخيص المريض ورعايته بشكل كبير. يتمثل التحدي الرئيسي في تطوير طريقة كشف يمكنها التمييز بدقة بين العقيدات الحميدة والخبيثة وتعمل بشكل فعال في ظل ظروف التصوير المختلفة. إن تطوير التكنولوجيا والاستثمار في تقنيات التعلم العميق في المجال الطبي يجعل من السهل استخدام التصوير المقطعي بالإصدار البوزيتروني (PET) والتصوير المقطعي المحوسب (CT). وبالتالي، تقدم هذه الورقة الكشف عن سرطان الرئة عن طريق تصفية صورة PET-CT، والحصول على منطقة الرئة ذات الاهتمام (ROI)، والتدريب باستخدام نماذج التعلم العميق للشبكة العصبية التلافيفية (CNN) للدفاع عن موقع العقيدات. تتكون مجموعة البيانات المحدودة من 220 حالة مع 560 عقيدة مع وحدات هاونسفيلد الثابتة (HU) المستخدمة لزيادة سرعة التدريب وحفظ البيانات. تتضمن النماذج المدربة CNN وDCNN وDCNN3 وVGG 19 وResNet 18 وInception V1 وInception-ResNet للكشف عن عقيدات الرئة. تُظهر التجربة أن التدريب عالي السرعة باستخدام VGG 19 يتفوق على بقية التعلم العميق، حيث يحقق الدقة والدقة والخصوصية والحساسية ودرجة F1 وIoU ومعدل FP بالتقسيم القياسي؛ 98.65 ± 0.22 و98.80 ± 0.15 و98.70 ± 0.20 و98.55 ± 0.18 و98.60 ± 0.16 و0.94 ± 0.03 و1.05 ± 0.22 على التوالي. علاوة على ذلك، تظهر نتائج التجربة معدل خطأ إجمالي إلى جانب التقسيم القياسي بين ± 0.04 إلى ± 0.54 موزعة على شروط الحساب.

الكلمات المفتاحية: الشبكة العصبية التكرارية التحويلية, صورCT, التعلم العميق, سرطان الرئة, العقيدات الرئوية